12-15-2006

Angle Resolved Photoemission Study of Epitaxial Chromium Dioxide Films

Daniel Borst
University of New Orleans

Angle Resolved Photoemission Study of Epitaxial Chromium Dioxide Films

A Thesis

Submitted to the Graduate Faculty of the
University of New Orleans
in partial fulfillment of the
requirements for the degree of

Master of Science
in
The Department of Physics

by

Daniel R. Borst

B.S. Purdue University, 2004

December, 2006

ACKNOWLEDGEMENTS

I would like to acknowledge my parents for their continuous love and support, and for pushing me in the right direction.

I would like to thank Dr. Ventrice for his guidance and motivation. I am grateful for his effort in acquiring the funding, time, and other resources required for my research and academic experience. I would also like to express my thanks to Dr. Arun Gupta for providing the samples for our research.

Thanks to my family and friends Heather, Jeff, Robin, Shalane, Ian, Giacamo, Emily, Jeremy, Bob, and Natalie for their friendship, encouragement, advice, and tolerance. I would also like to thank Michelle and Christy for providing the necessary caffeine for my master's thesis and rapidly approaching deadlines, and Sandra for sharing my lack of enthusiasm for paperwork.

I would like to thank Dr. Sprunger, Dr. Losovich, and Dr. Geisler for their encouragement and expertise.

I extend my gratitude to Purdue University, the U.N.O and L.S.U physics departments for the education provided throughout my academic career.

TABLE OF CONTENTS

LIST OF FIGURES

LIST OF TABLES

ABSTRACT

Chromium dioxide is predicted to be a half-metallic oxide. The electronic properties of the surface region of CrO_2 have been studied by performing angle-resolved ultra-violet photoelectron spectroscopy (ARUPS) measurements on epitaxial CrO_2 films. The CrO_2 thin films were deposited on (100) and (110) – oriented TiO_2 substrates by chemical vapor deposition. Previous measurements of the transport properties of devices made from epitaxial CrO_2 films have shown very little spin polarization. Possible sources of this low yield are a surface Cr_2O_3 phase and/or surface contamination. The effects of sputtering the CrO_2 films to remove the outer layer of Cr_2O_3 and any surface contaminants and of annealing the films in oxygen to heal surface were examined. The ARUPS spectra of the CrO_2 films have been compared to epitaxial Cr_2O_3 films prepared on Pt(111). In addition, low energy electron diffraction patterns of the sputtered and annealed CrO_2 films have been prepared indicating that the surface remains in a CrO_2 phase.

1. INTRODUCTION

1.1 Motivation

The recently discovered phenomenon of half-metallic behavior has attracted considerable attention in the context of rapidly emerging fields of spin-polarization electronics (spintronics). Half-metals simultaneously exhibit conducting and insulating properties, with the unusual effect of being metallic for electrons sharing the same spin direction, and insulating for electrons with the opposite spin direction [8]. The resulting magnetic moment is already being explored for use in semiconductor and nanoscale technologies such as magnetic random access memory (MRAM), and spin momentum transfer (SMT). In particular, CrO_2 films are attractive due to the predicted high spin-polarization near the Fermi level. Spin polarized conduction studies are yielding promising results for device fabrication in speed, size, selectivity, and power as the boundaries of more traditional methods are being realized.

The effect of magnetoresistance, or the ability for a substance to change its resistance based on applied magnetic fields, is also being explored. Giant magnetoresistance (GMR) offers the possibilities of memory devices with superior storage capabilities with the advantage of being immune to power interruptions and ionizing radiation – an appealing prospect for military and space applications. Tunnel magnetoresistance (TMR) is another developing area in electron control, based on the crystal's magnetic bias as theory indicates improved semiconductor properties.

1.2 Background Information and Previous Work

Although a number of theoretically predicted half-metallic materials have been identified, CrO_2 is the only material for which half-metallicity has been experimentally

confirmed. The metastable nature of the film frequently results in the formation of a natural Cr_2O_3 on the CrO_2 surface, because it is, thermodynamically, much more stable. High-resolution microscopic studies have verified the occurrence of the lattice matched hexagonal corundum structure of Cr_2O_3 on the CrO_2 surface [10,13]. It is questionable as to what causes the spontaneous growth of the undesired layer, or when it is formed. Because it is metastable, CrO_2 will irreversibly reduce to Cr_2O_3 at high temperatures and atmospheric pressure. As expected, temperature constraints must be considered when dealing with metastable heterostructures. It is unclear whether the reduced layer forms immediately after film growth termination or after exposure to the atmosphere [10,13].

Theoretical studies predict the CrO_2 half-metal to have a full spin-polarization of 100% as shown in Fig. 1.1. Samples examined in previous studies grown by chemical vapor deposition (CVD) with chromyl chloride (CrO_2Cl_2) as a liquid precursor, yielded atomically smooth films with spin polarizations of 98.4% [13]. Magnetization and resistivity measurements were comparable to the fabrication group's more cumbersome methods involving CrO_3 powder as a solid precursor. As such, CVD is the preferred fabrication technique for CrO_2 crystal growth for most CrO_2 spin-polarization research [9].

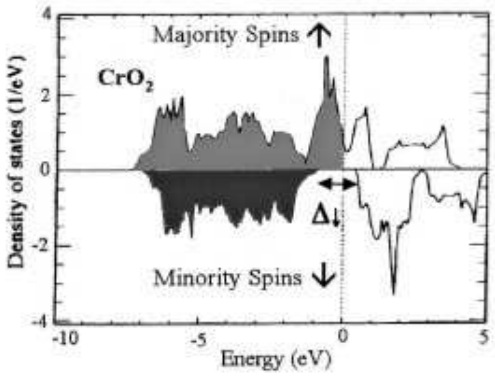

Fig. 1.1 *Spin polarization of the density of states of CrO_2 [8]*

1.3 Present Work

The present study focuses on the properties of epitaxial CrO_2 thin films grown on TiO_2 as a template. TiO_2 is an excellent foundation for epitaxial growth since the substrate cuts of various orientations are available and the lattice mismatch is only about 4%. From our LEED and photoemission measurements that were taken after a variety of sputtering and annealing cycles, the films show a surprisingly stable film structure with no indications of major surface reduction. Photoemission measurements taken demonstrate that the oxygen and chromium concentrations maintain their initial atomic ratio under the conditions used in these experiments and are not as sensitive as anticipated.

Hydrocarbon contamination can become prevalent at some point during the film growth, atmosphere exposure, or vacuum analysis. To reduce the presence of oils and lubricants, a dry scroll pump was temporarily implemented to possibly provide insight into the hydrocarbon's origin. The hydrocarbon contamination showed no attenuation and appears to be present before vacuum analysis. As with earlier studies, a shift in the Fermi level of CrO_2 occurs after sputtering, which is probably due to slight changes in the stoichiometry of the surface. All photoemission and LEED measurements were taken at the CAMD synchrotron in Baton Rouge, Louisiana. A picture of the CAMD experimental hall is shown in Fig. 1.2.

Fig. 1.2 *CAMD Experimental Hall*

2. EXPERIMENTAL DETAILS

2.1 Ultra-High Vacuum

Clean surfaces are generally very reactive towards impinging particles from residual gas mixtures similar to that existing in normal atmospheric conditions. The sensitivity of clean surfaces as such requires a well-controlled environment in which the effects of undesirable surface contamination reactions and alterations can be minimized. By maintaining a clean contamination free surface, it can be studied with the advantage of obtaining repeatable results. Most systems are equipped with a number of measurement devices capable of controlling other conditions, such as temperature and deposition rates. Kinetic gas theory indicates that the number of particles colliding with a surface per unit time and area is determined by

$$\left(\frac{dn}{dt}\right)_s = \frac{1}{4} N_g \overline{v} \tag{2.1.1}$$

where N_g is the number of gas molecules per cm^3 and $\overline{v}$ is their average thermal velocity. It then follows that

$$\left(\frac{dn}{dt}\right)_s = N_g \sqrt{\frac{RT}{2\pi M}} \approx 3.5 \cdot 10^{22} \frac{P}{\sqrt{MT}} \left[cm^{-2} s^{-1}\right] \tag{2.1.2}$$

where

R = gas constant
T = absolute temperature
M = molecular weight
and P = gas pressure in Torr.

Assuming a monolayer capacity of $3.5 \cdot 10^{14}$ particles/cm^2, at temperature T = 300 K, and a molecular weight of M = 28, eq. (2.1.2) yields

$$\left(\frac{dn}{dt}\right)_s \approx 10^6 \cdot P\left[\text{monolayers/s}\right]. \qquad (2.1.3)$$

Consequently, at 760 Torr (atmospheric conditions) the number of molecules needed to assemble a monolayer is offered to a surface almost every nanosecond. At a pressure of 10^{-6} Torr (standard high vacuum conditions) the time necessary for a surface to build a monolayer is reduced to 1 second. Monolayer construction also depends on the probability that impinging molecules will be accepted, which is called the sticking coefficient 's'. This is quite often close to unity for reactive surfaces such as Si. It is clear that much lower pressures are critical for surface research [4].

Ultra-high vacuum systems are capable of achieving pressures less than 10^{-10} Torr, which is ultimately determined by gases emitted from the materials used to build the apparatus itself [4]. Since most spectroscopic techniques are also capable of detecting molecules in the gas phase, the number of particles present on the surface should substantially exceed those present in the gas phase immediately above the surface [6].

The mean free path, λ, is defined as the average distance traveled by a particle between collisions

$$\lambda = \frac{kT}{\sqrt{2}\,P\sigma} \qquad (2.1.4)$$

where

k = Boltzmann's constant (= 1.38 x 10^{-23} J/K)
T = temperature [K]
P = pressure [N/m^2]
σ = collision cross section [m^2].

Low-pressure atmospheres allow the use of various electron- and ion-based measurement techniques by creating large λ by (relative to experiment apparatus), thus avoiding gas

phase scattering and allowing relatively uninterrupted particle flow to and from the surface [11].

2.2 Angle-Resolved Photoemission

Photoemission is the release of electrons from a material by means of a photon in/electron out energy transfer process. Photoemission techniques are capable of extracting atomic information about surfaces through the use of this relationship by analyzing the kinetic energy of photoemitted electrons. Photoelectron spectroscopy for material studies is typically broken into two branches, classified by the source of exciting radiation: ultraviolet and X-ray photoelectron spectroscopy (UPS and XPS, respectively). Taking advantage of these different radiation energies provides valuable information about electron binding energies within a material. In UPS, ultraviolet radiation (<200 eV) is used to examine valence electron properties, while the higher energy soft X-rays (200-5000 eV) employed in XPS can be used to probe deeper into the atom, revealing core level electron properties [2]. By examining the binding energies of electrons of various materials, spectroscopy exposes not only the atoms present in a material, but also their relative ratio, or stoichiometry, thus identifying molecules within the material. XPS and UPS spectra for samarium is shown in Fig. 2.1.

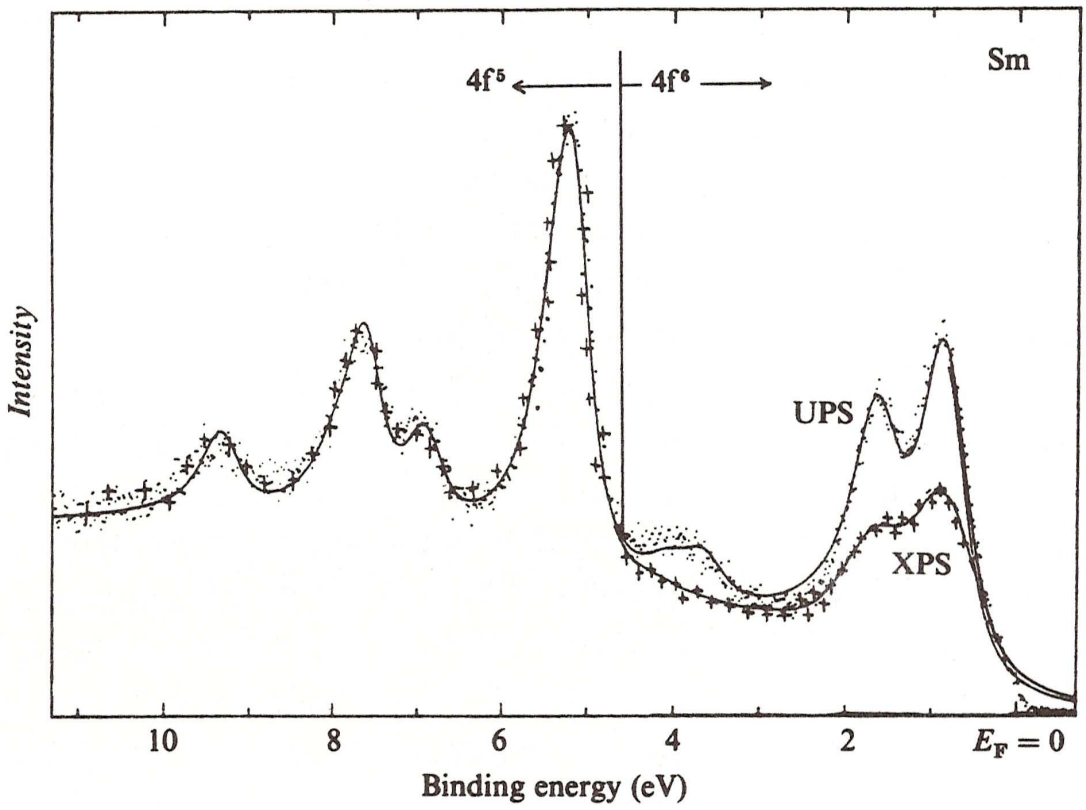

Fig. 2.1 *Photoemission energy density diagram from the f-shell of samarium. The UPS spectrum is more surface sensitive than the XPS results [2].*

Both methods ionize secondary electrons beneath the surface as a consequence of the light source being able to penetrate farther into the surface than the mean free path of the primary electrons, resulting in inelastic scattering, and creating a background signal onto which the surface signal is constructed. The inelastic mean free path of electrons in a solid modeled as a free electron gas is shown by the dashed curve in Fig. 2.2 [2].

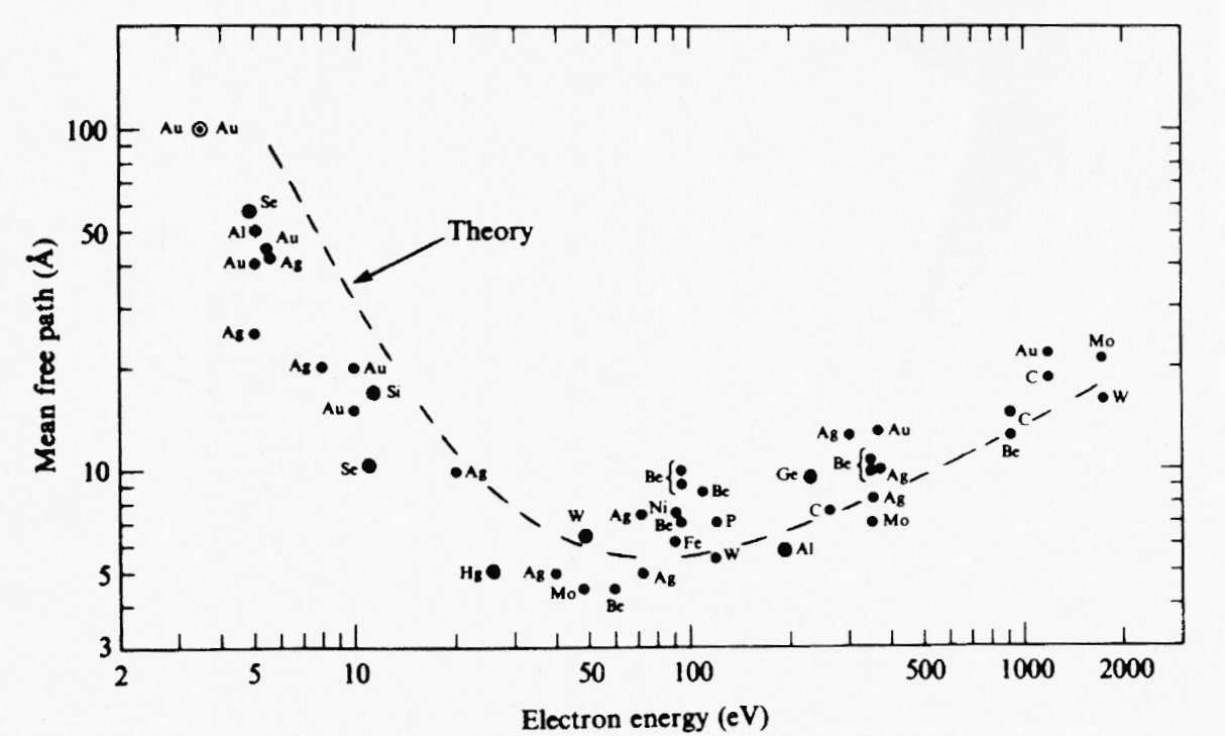

Fig. 2.2 *Universal curve of electron mean free path [2]*

The photoionization process can be described by considering momentum transfers at the atomic level and making use of the conservation of energy principle. Einstein and Planck determined that the energy of a photon is proportional to the frequency of the radiation, and is given by Einstein's relation

$$E = h\nu \tag{2.2.1}$$

where

h = Planck's constant (6.62×10^{-34} J · s)
ν = frequency of radiation [Hz].

Conservation of energy requires that the kinetic energy of the escaping photoelectron added to the amount of energy required to release the electron, or binding energy, is equal to the energy of the incoming photon, or

$$E_{\text{kin}} = h\nu - E_{\text{b}} - q\varphi \tag{2.2.2}$$

where the binding energies of electrons are usually referenced to the Fermi level. Therefore there is a barrier for photoemission $W = q\varphi$ that results for the work function φ of the crystal. This describes a photon in/electron out process, whereby the specific electron binding energies provide information about the atomic arrangements. Several photoemission scenarios are illustrated in Fig. 2.3.

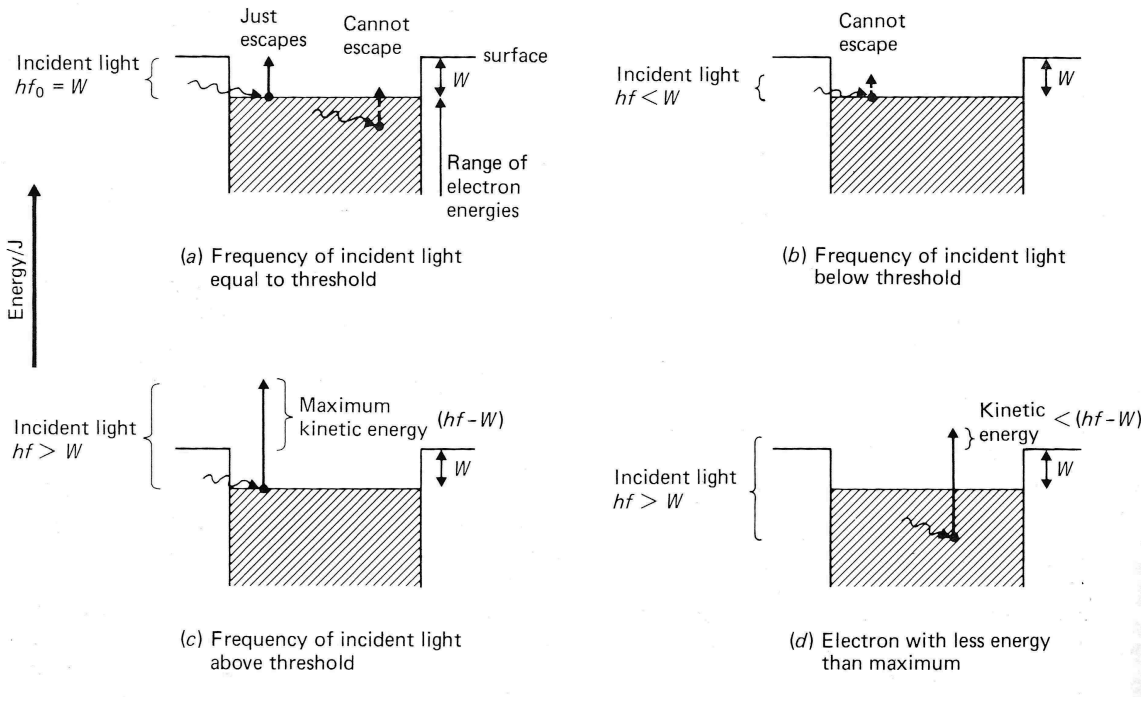

Fig. 2.3 *The emission of photoelectrons [1]*

A schematic of the photoemission experimental geometry is shown in Fig. 2.4. Since the photoelectron's kinetic energy is measured at the spectrometer, its measured kinetic energy is referenced to the work function of the spectrometer, not the sample. This is shown in Fig. 2.5.

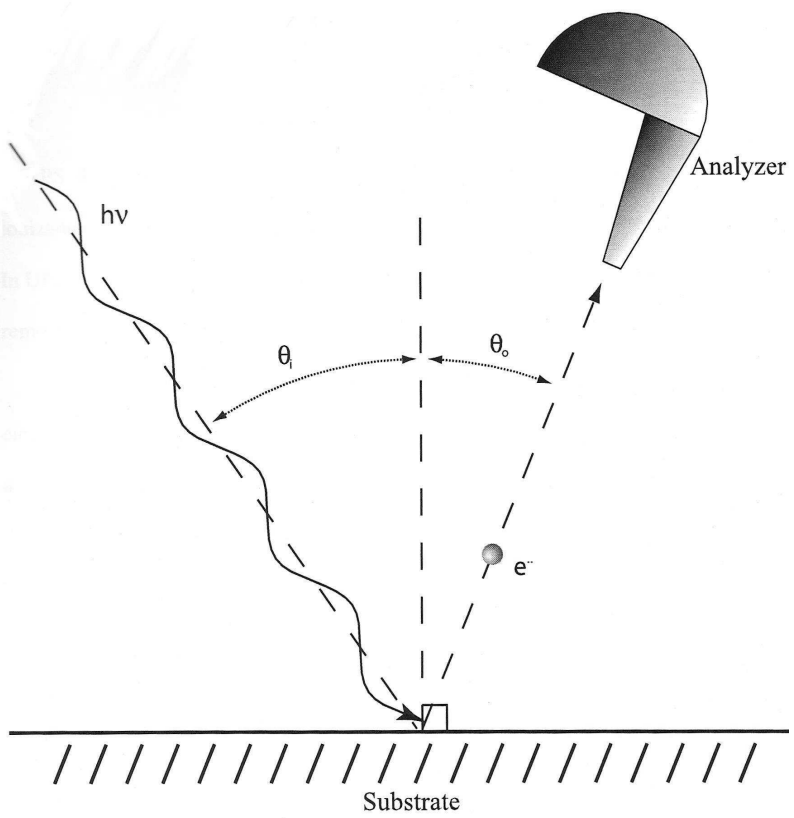

Fig. 2.4 *Photoionization diagram*

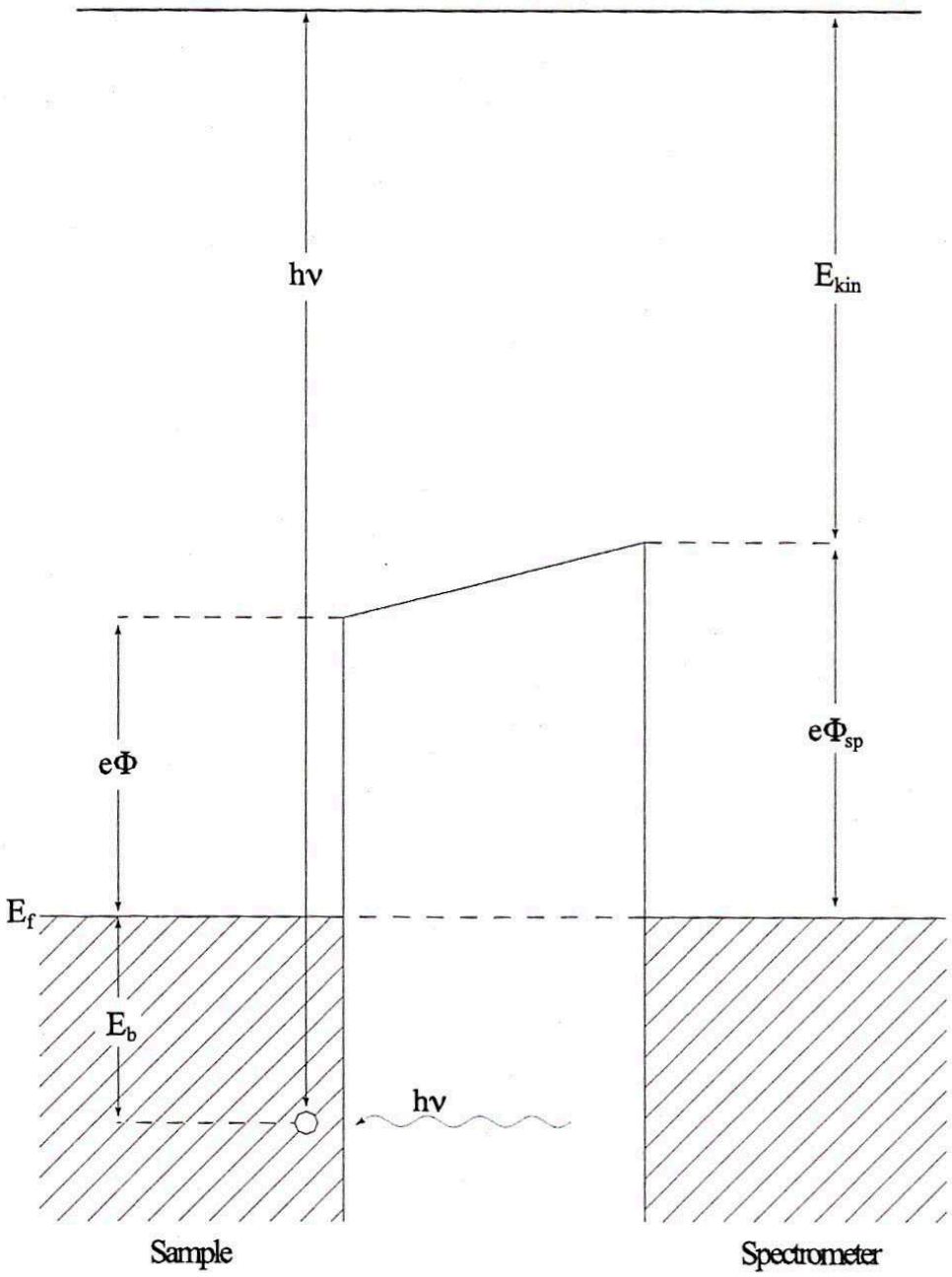

Fig 2.5 *Energy level diagram for photoelectron spectroscopy [4]*

2.3 Low Energy Electron Diffraction (LEED)

LEED analysis involves the use of a beam of electrons of well-defined energy incident normal to a surface. Electrons from the beam are scattered back toward a phosphor coated screen creating a diffraction pattern, rendering information about the spacing, symmetry, and alignment of the sample's unit cell and geometric structure. A schematic of a LEED optics system is shown below.

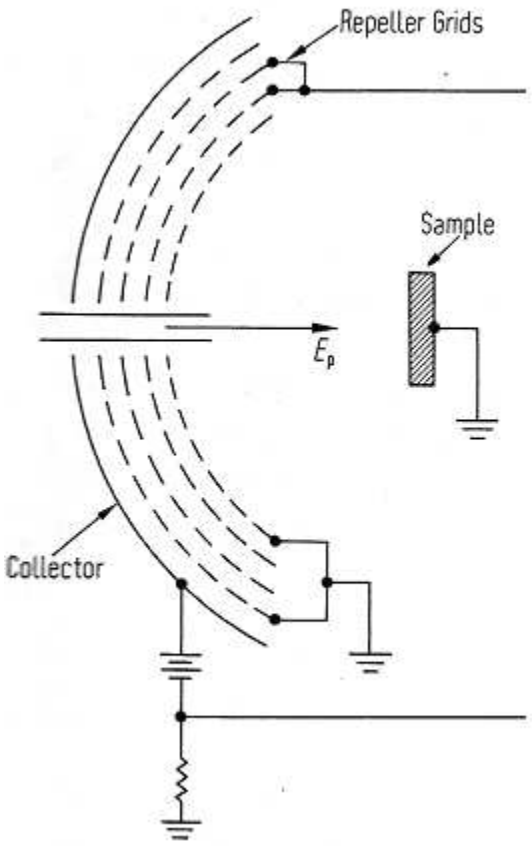

Fig. 2.6 *Typical schematic of a 4 grid LEED system as a retarding field analyzer [4]*

With the appropriate wavelength, the backscattered electron beams from well-ordered surfaces generate a pattern identifying specific molecular orientations. Wave-particle duality theory indicates that the beam of electrons may be regarded as electron

waves normal to the sample. Surface atoms are treated as a plane of point scatterers, as shown in figure 2.7.

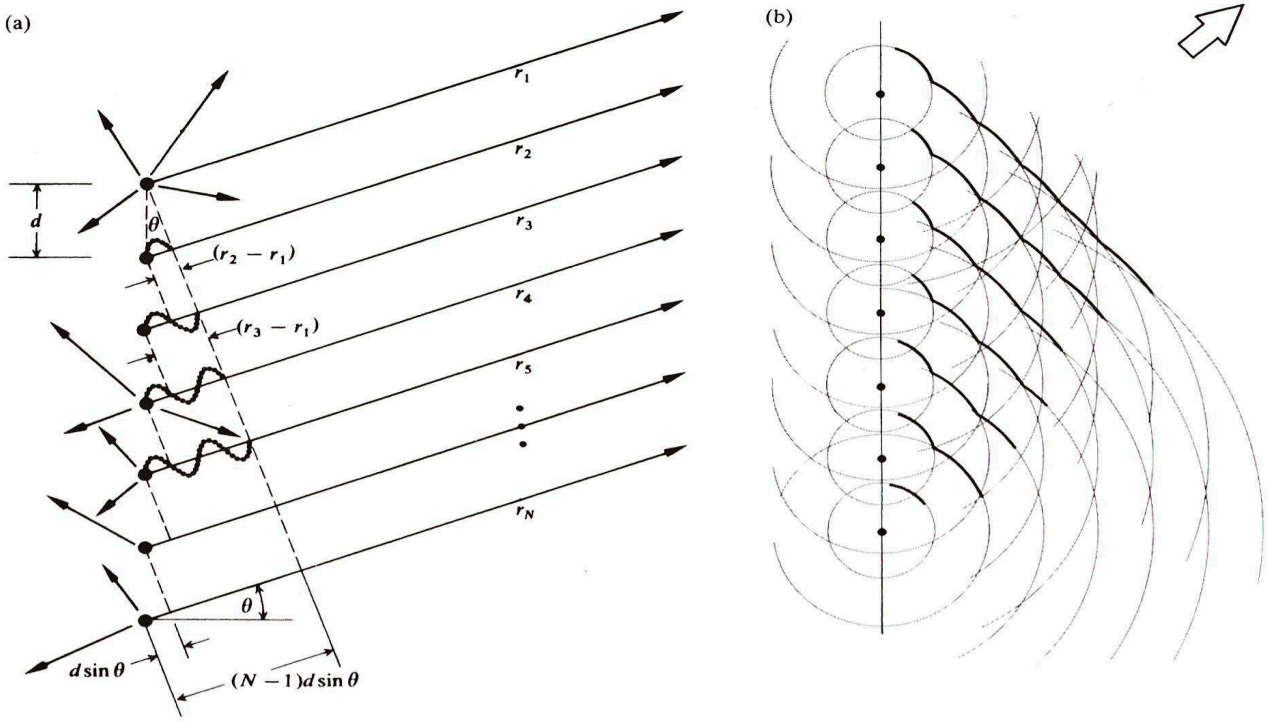

Fig 2.7 *A linear array of in-phase coherent oscillators [12]*

The de Broglie wavelength, λ, written in terms of Planck's constant, *h*, and the electron momentum *p*, is defined as

$$\lambda = \frac{h}{p} \ . \tag{2.3.1}$$

The relationship can be rewritten in terms of the elementary electron charge, *e*, electron mass, *m*, and the acceleration voltage, *V*, as

$$\lambda = \frac{h}{\sqrt{2m \cdot e \cdot V}} \ . \tag{2.3.2}$$

Thus, electron energies on the order of 150 eV have a wavelength of approximately 1 Å, which is suitable for diffracting ordered crystal arrays. Electrons employed in LEED are

typically in the range of 10 – 475eV, corresponding to a wavelength range of 3.9 to .56 Å. Low energy electrons are ideal for surface analysis as they penetrate only the first few layers (~ 5 Å) of a substrate. As a result, the emerging diffraction patterns characterize the reciprocal lattice, the projection of reciprocal vectors defined by two-dimensional surface vectors.

The von Laue formulation assumes that sets of atoms in a Bravais lattice radiate the incident radiation at the same frequency in all directions. As a consequence, the radiation interferes constructively, producing the diffraction maxima. The geometry of two scattering centers separated by a distance *d* where the incident and scattered radiation have wave vectors $\vec{k}$ and $\vec{k}'$, respectively, in the directions of the unit vectors $\hat{e}$ and $\hat{e}'$, respectively ($\hat{e} \equiv \vec{k}/|\vec{k}|$,etc.). Thus, $k = 2\pi\,\hat{e}/\lambda$ and $k' = 2\pi\,\hat{e}'/\lambda$. This is diagrammed in the figure below.

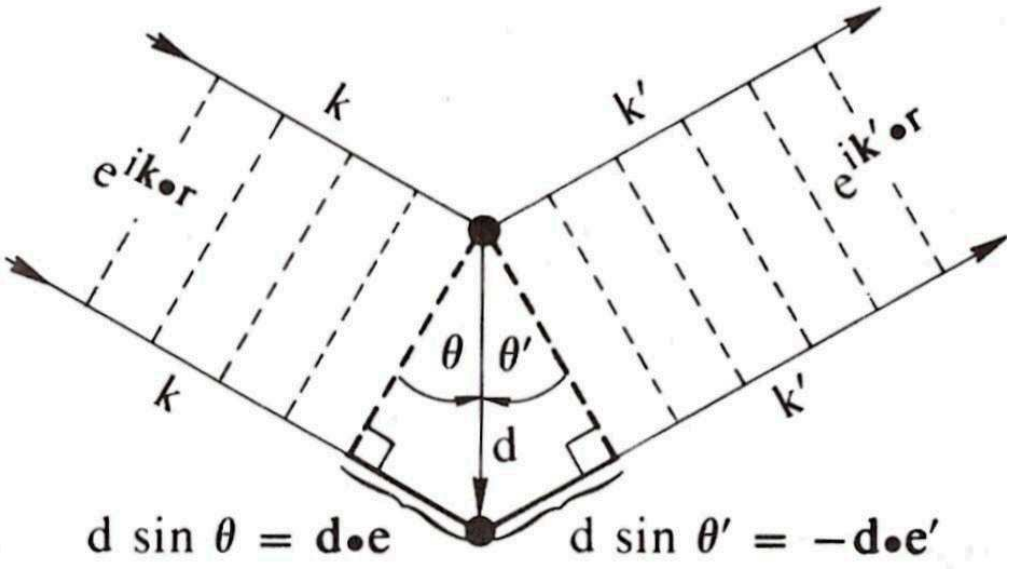

Fig. 2.8 *The path difference for two arbitrary scattering centers [3]*

The path difference is

$$d\sin\theta + d\sin\theta' = \vec{d}\cdot(\hat{e} - \hat{e}') \tag{2.3.3}$$

and

$$\vec{d}\cdot\left(\vec{k} - \vec{k}'\right) = 2\pi n \tag{2.3.4}$$

where n is any integer. Therefore, when the path difference is an integral number, n, of wavelengths then constructive interference occurs. By using the Bravais translation vector it is possible to describe the constructive interference from an entire plane of scattering elements, as illustrated in Fig. 2.7 [12]. The translation vector for a 3–Dimensional crystal is defined as

$$\vec{t_m} = m_1\vec{a} + m_2\vec{b} + m_3\vec{c} \tag{2.3.5}$$

where $\vec{a}$, $\vec{b}$, and $\vec{c}$ are three arbitrary, independent vectors, and m_i is any integer. Then

$$\vec{t_m}\cdot\left(\vec{k} - \vec{k}'\right) = 2\pi n. \tag{2.3.6}$$

This expression can also be written in the equivalent form

$$e^{i\left(\vec{k}-\vec{k}'\right)\cdot\vec{t_m}} = 1\,. \tag{2.3.7}$$

The set of wave vectors $\vec{K} = \vec{k} - \vec{k}'$ that satisfy the above equation is called the reciprocal lattice, and is generated by three primitive reciprocal lattice vectors

$$\vec{a}^{\,*} = 2\pi\frac{\vec{b}\times\vec{c}}{\vec{a}\cdot\left(\vec{b}\times\vec{c}\right)}\,, \qquad \vec{b}^{\,*} = 2\pi\frac{\vec{c}\times\vec{a}}{\vec{a}\cdot\left(\vec{b}\times\vec{c}\right)}\,, \qquad \vec{c}^{\,*} = 2\pi\frac{\vec{a}\times\vec{b}}{\vec{a}\cdot\left(\vec{b}\times\vec{c}\right)} \tag{2.3.8}$$

where $\vec{a}$, $\vec{b}$, and $\vec{c}$ are the primitive lattice vectors. For example, for a simple-cubic Bravais lattice, with a primitive cell of size *a*,

$$\vec{a} = a\hat{x}, \qquad \vec{b} = a\hat{y}, \qquad \vec{c} = a\hat{z} \tag{2.3.9}$$

the reciprocal lattice vectors are

$$\vec{a}^* = \frac{2\pi}{a}\hat{x}, \qquad \vec{b}^* = \frac{2\pi}{a}\hat{y}, \qquad \vec{c}^* = \frac{2\pi}{a}\hat{z} \tag{2.3.10}$$

Fig. 2.7 shows plane waves propagating from a linear array of in-phase coherent oscillators in the direction of the reciprocal lattice vectors, resulting in a number of diffraction spots, which construct the interference pattern [7,3,5]. Sample LEED patterns are shown in Fig. 2.9.

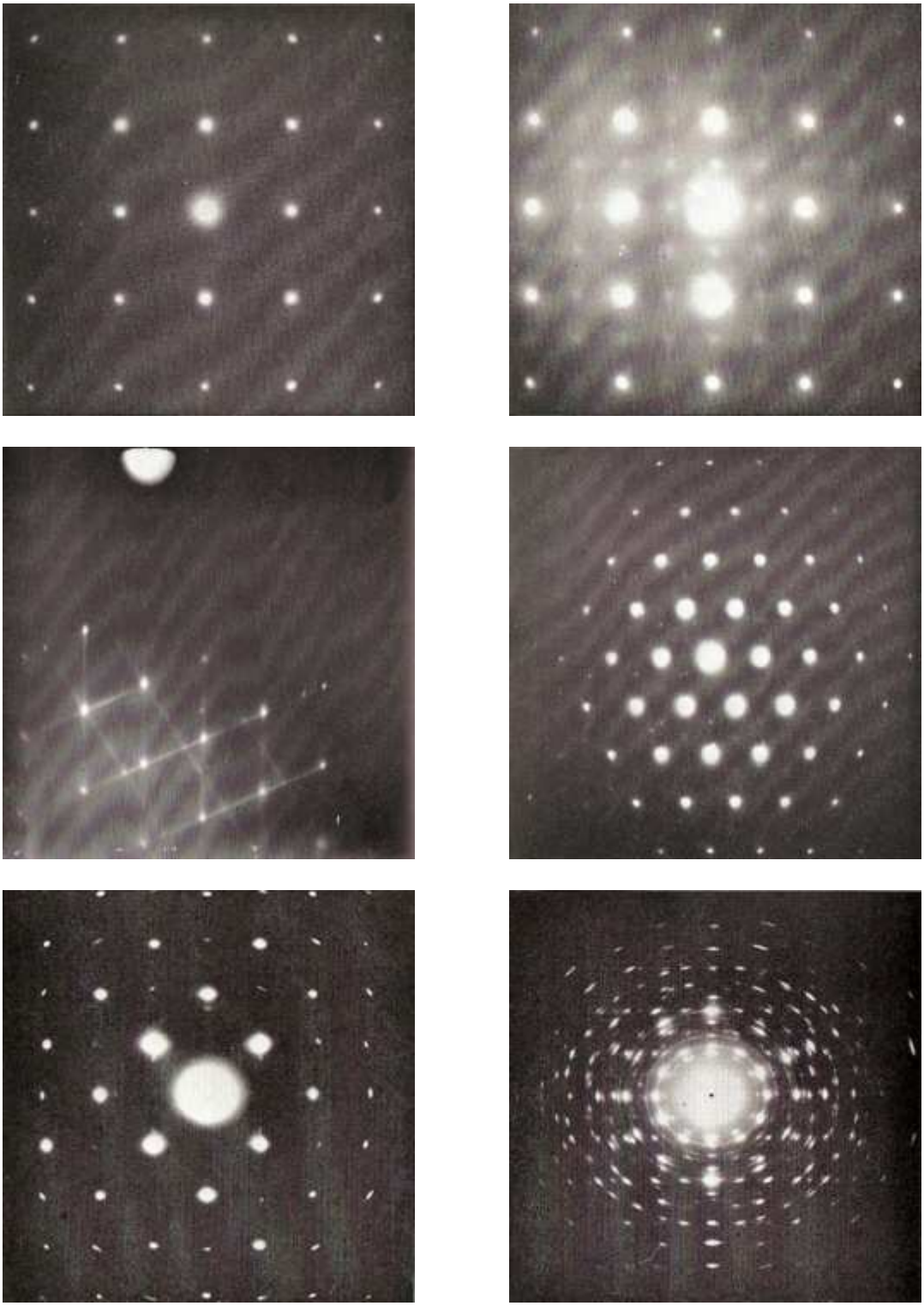

Fig 2.9 *Several LEED pattern examples [14]*

2.5 Sample Preparation

The present study makes use of a variety of sputtering and annealing cycles under vacuum conditions for surface preparation. Chromium dioxide films were sputtered with argon for times ranging between 5 and 30 minutes, stripping the surface of its outermost layers, and presumably contaminants, by introducing high voltages capable of accelerating the argon ions admitted into the vacuum chamber toward the target film. The damaged surface subsequently is 'repaired' by annealing at high temperatures (after restoring UHV conditions), by which amorphous regions recrystallize [2]. However, annealing can also result in driving impurities to the surface, resulting in contamination of the upper layers. This effect is seen in our results, and is clearly a result of the liquid precursor. As such, this procedure is most effective if repeated several times. A picture of the CrO_2(100) crystal mounted on a sample holder is shown in Fig. 2.10.

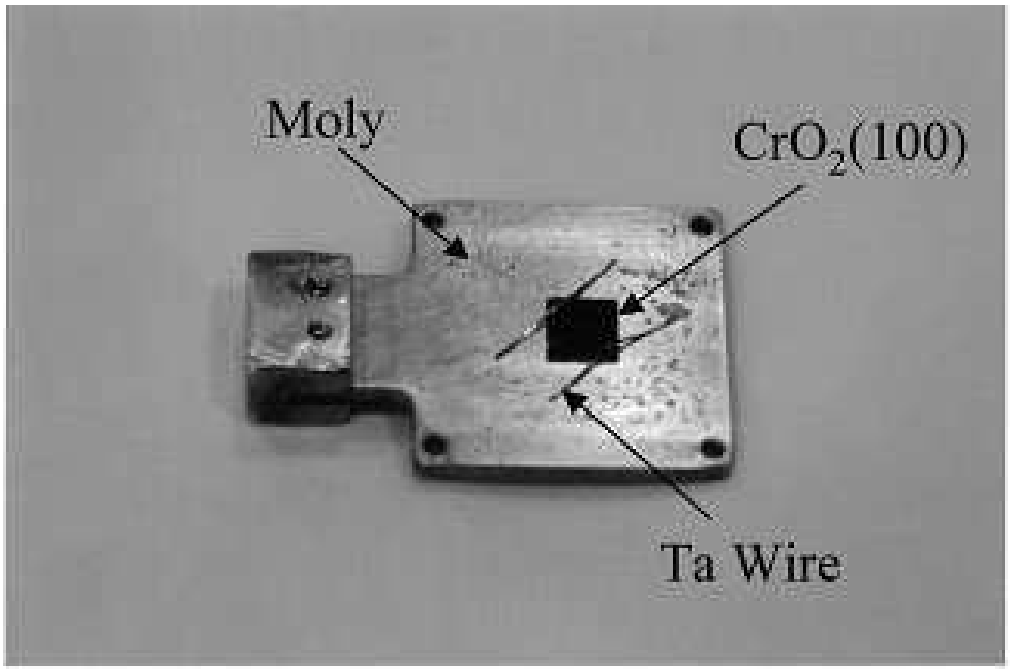

Fig. 2.10 *Photograph of sample holder and crystal*

The CrO_2 films were grown at the Univ. of Alabama by Prof. Arun Gupta's research group using a chemical vapor deposition (CVD) technique with a CrO_2Cl_2 liquid precursor. The deposition reactor used consists of a quartz tube placed inside a furnace and kept at 400º C. After being cleaned with a number of organic solvents and dilute hydrofluoric acid, the TiO_2 substrates onto which the CrO_2 films are to be grown are placed on a glass susceptor. The precursor is placed into a bubbler and held at 0º C. The flow rate of the oxygen carrier gas is 40 cc^3/min, resulting in a deposition rate of 72 Å/min. The procedure results in epitaxial films yielding actual spin polarizations near 100% [9].

3. RESULTS AND DISCUSSION

The theoretically predicted 100% spin polarization of CrO_2 has, so far, not been a reality in the field of epitaxial CrO_2 device fabrication, as a possible result of crystal reduction due to its' meta-stable nature and/or surface contamination. The meta-stable nature of CrO_2 predicts eventual crystal reduction into the more stable form of Cr_2O_3. It is possible to determine the occurrence of reduction and surface contamination by using photoemission comparison techniques. By determining the relative ratio of elements for photoemission results for the unknown chromium oxide states and comparing them to known results it is possible to determine the molecular identity of the epitaxial film, and possibly isolate the source of such low spin polarization yields for device fabrication.

3.1 Spin-resolved Electronic Structure Calculations

Electronic structure calculations performed by Dr. Johannes van Ek predict a conductive magnetic moment for CrO_2, suggesting a minority electron concentration above the Fermi level, and a majority electron concentration below. The predicted density of states for the reduced chromium oxide state of Cr_2O_3 indicates a semiconductor with electron spins of both directions above the Fermi level, and does not show any sign of spin polarization, making it suspect for the unimpressive device transport properties observed. The predicted density of states results for CrO_2 and Cr_2O_3 are illustrated in figures 3.1 and 3.2, respectively. Electrons above the Fermi level for CrO_2 are predominantly minority electrons of the same spin, predicting a near 100% spin polarization for conducting electrons – a nearly ideal half-metal. On the other hand, the symmetry of majority and minority electrons for energies above the Fermi level for Cr_2O_3 suggests a non-magnetic crystal.

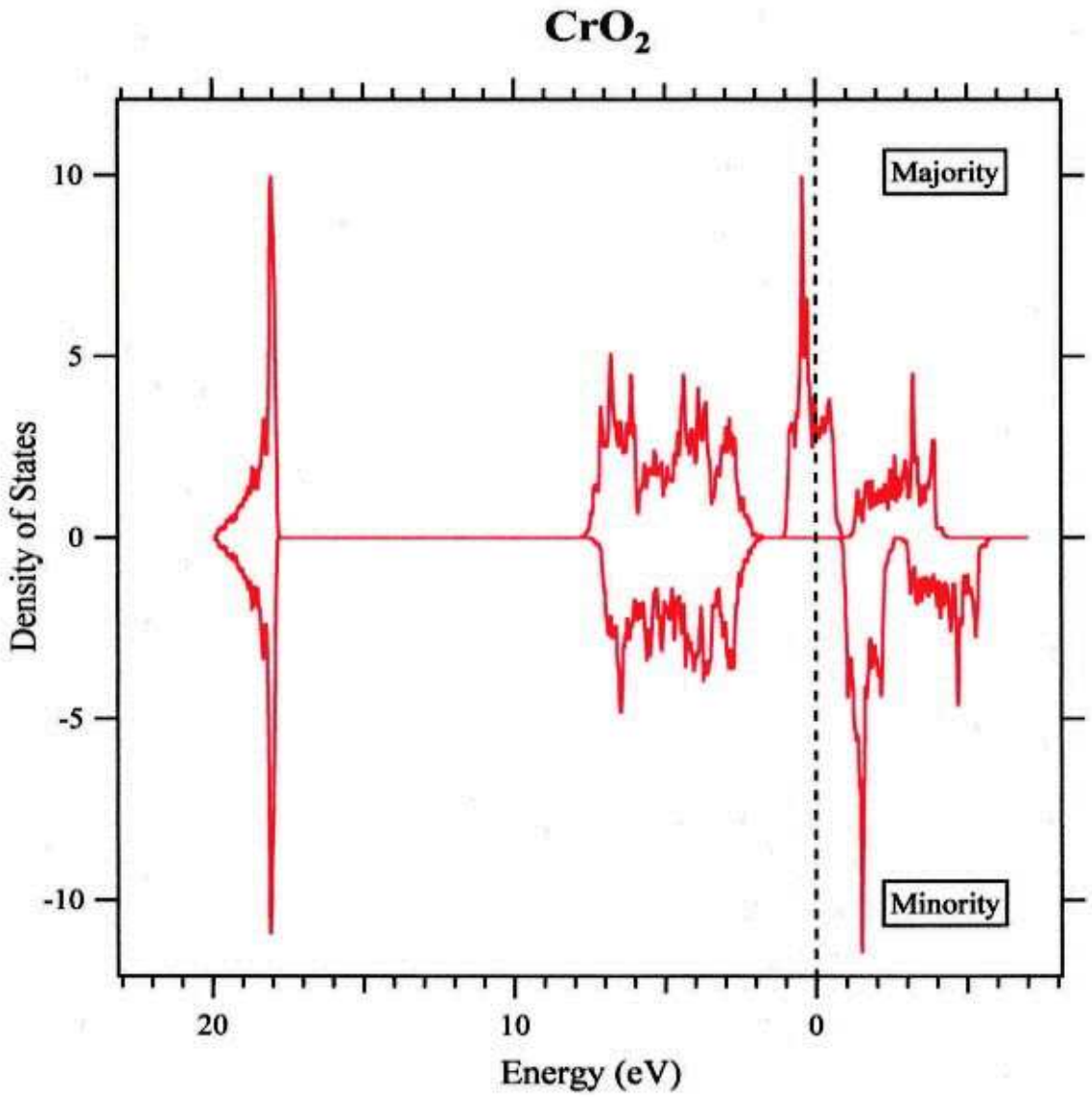

Fig. 3.1 *Calculated spin-resolved density of states for CrO_2*

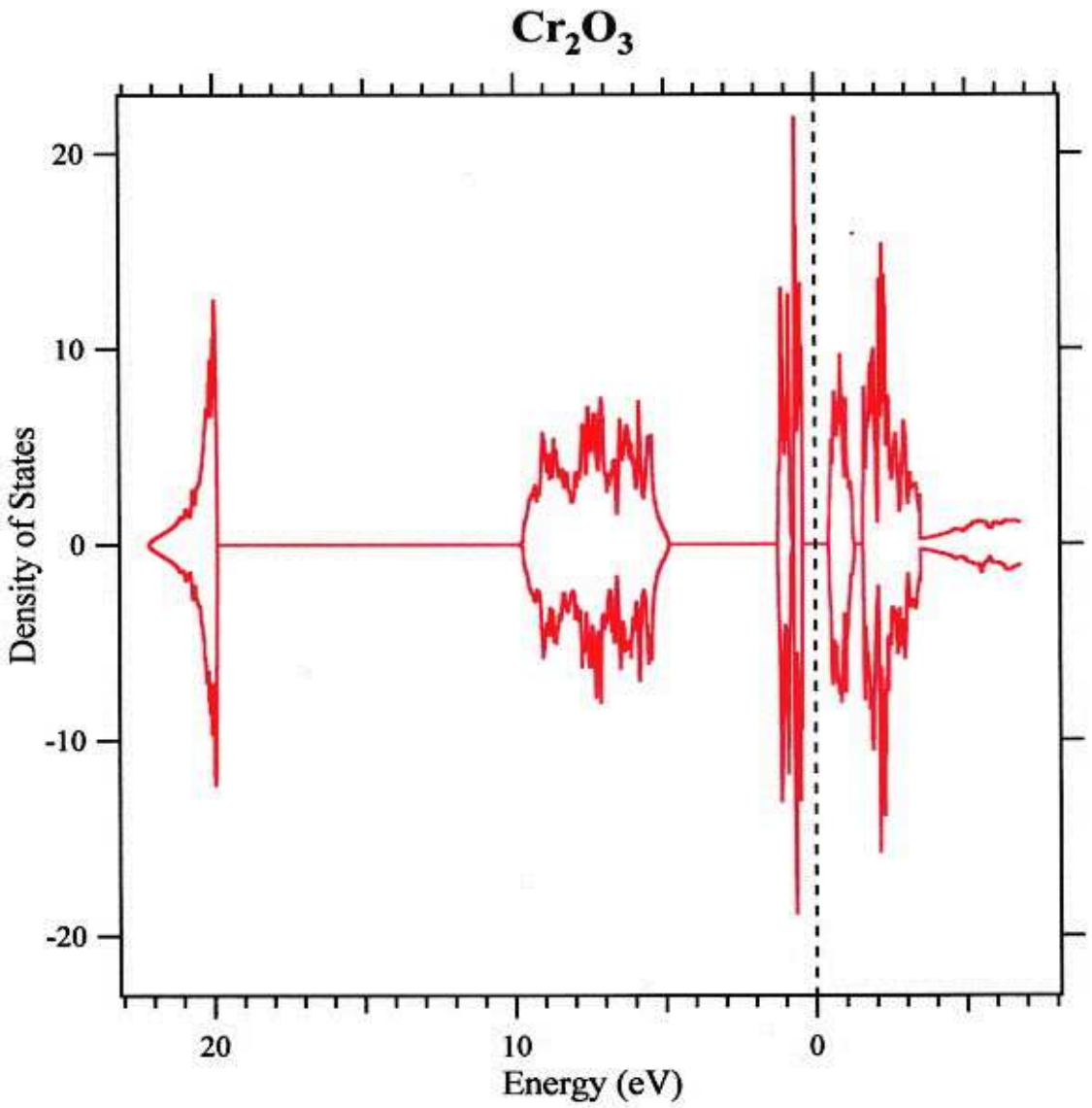

Fig. 3.2 *Calculated spin-resolved density of states for Cr_2O_3*

Since the photoemission measurements taken are not spin-resolved, comparisons must be made relative to the total density of states – the sum of majority and minority density of states multiplied by the Fermi function [10]. The total density of states for CrO_2 and Cr_2O_3 are shown in figures 3.3 and 3.4, respectively. Calculated results for CrO_2 suggest occupied states above the Fermi level, predicting a metallic nature, while

Cr_2O_3 predictions indicate insulating characteristics, as there are no occupied states visible above the Fermi level.

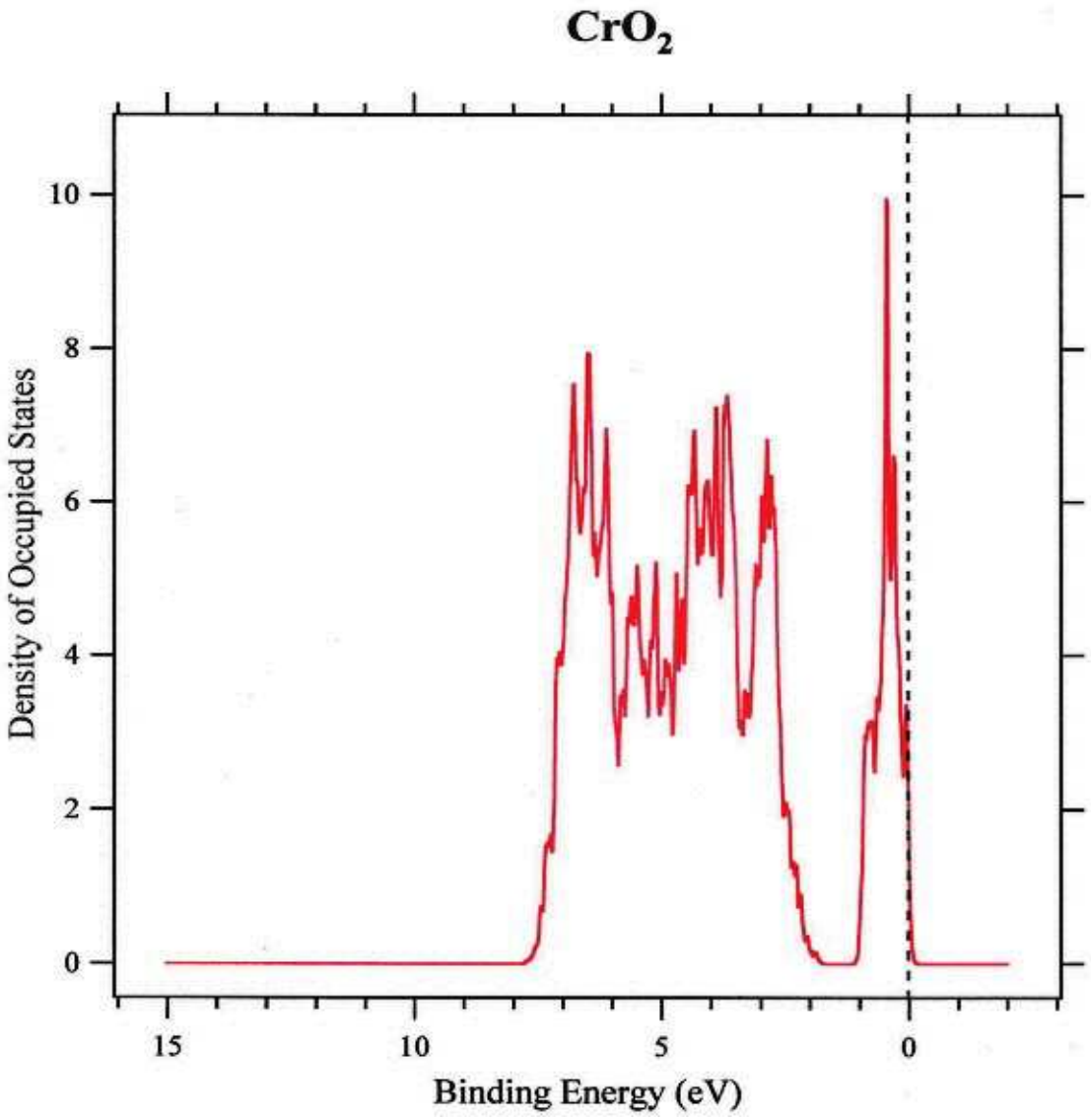

Fig 3.3 *Total density of states for CrO_2*

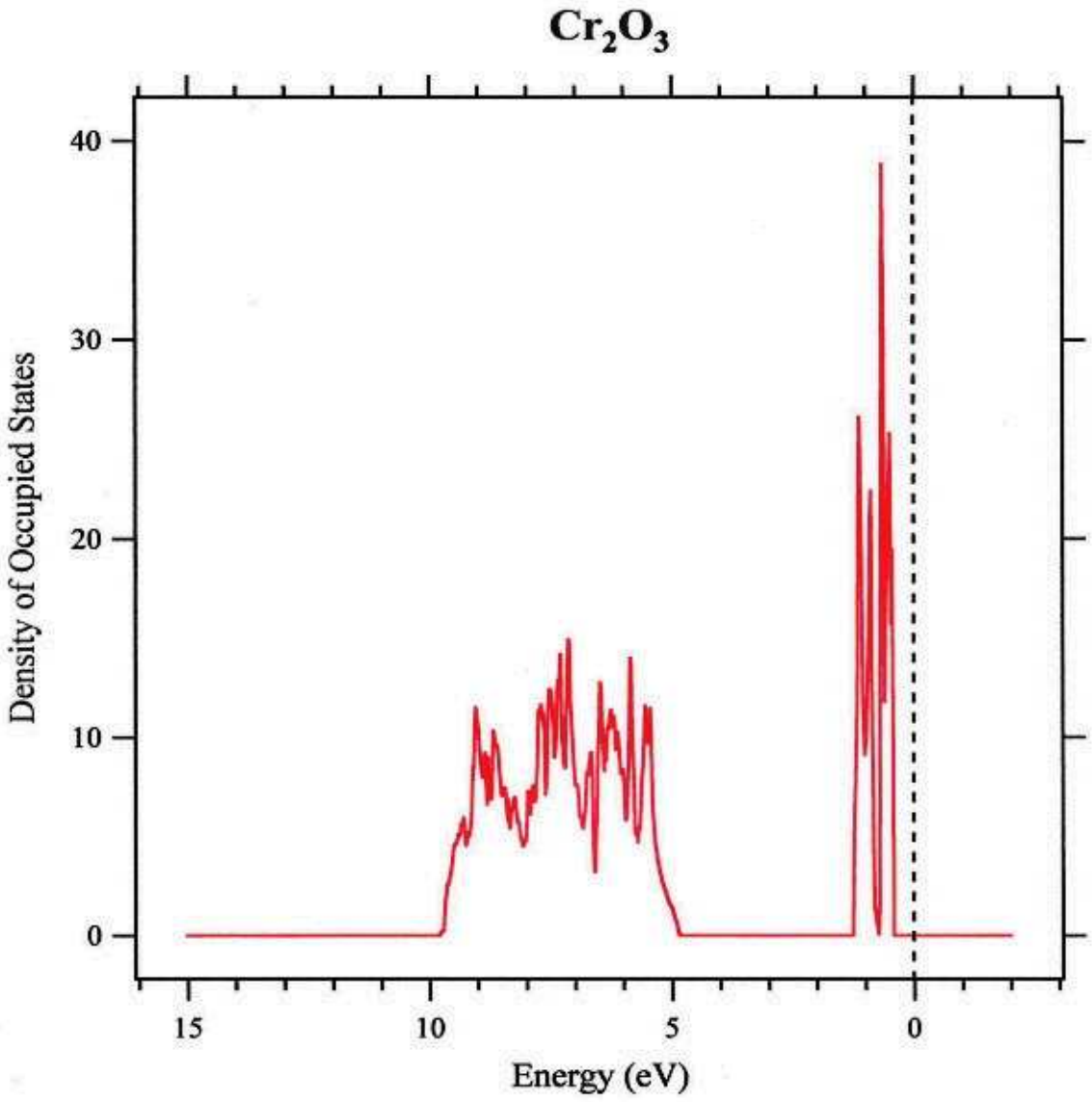

Fig 3.4 *Total density of states for Cr_2O_3*

3.2 Angle-resolved Ultraviolet Photoemission Measurements

All photoemission measurements from CrO_2 were taken at the TGM/3m beamline of the CAMD synchrotron in Baton Rouge, Louisiana, with light at an angle of incidence (ψ_i) of 45º. Core and valence emission measurements were taken with polarized light intensities of 120 eV and 75 eV, respectively. Spectra shown are presented as electron count intensities normalized to the current in the synchrotron ring versus binding energy relative to the Fermi level. The Cr_2O_3 spectra were taken at the NSLS synchrotron at Brookhaven by Robbert et al., for a thin film grown on platinum and are displayed at the top of each plot for convenient comparison [10]. Since the thermocouple is mounted on the manipulator block, not directly on the crystal, temperatures are only accurate to ~100º C.

3.2.1 CrO_2(100)

Spectra taken for CrO_2 cores at a photon energy of hν = 120 eV are shown in Fig 3.5. Before film preparation, the molybdenum 4p electrons from the sample holder and tantalum 4f electrons from the wires fixing the sample to the holder are visible. After annealing at 250º C in oxygen, the chromium oxide film begins to dominate the spectra, and the presence of the chlorine 3s electrons from the liquid precursor is slightly detected. This effect is observed before sputtering and is a result of residual impurities being driven to the surface from annealing. Sputtering of the surface results in the detection of distinct O-2s and Cr-3p peaks. Annealing at 450º C in 10^{-6} Torr of O_2 results in a slight increase of the chromium and oxygen peaks, and the peaks appear to be much more defined about their appropriate binding energies. None of the spectra appear to resemble the Cr_2O_3 phase included at the top of the chart – a more rigorous numerical

analysis distinguishing chromium dioxide phases involving peak integration is included in section 3.4.

Valence emission measurements taken at a photon energy of 75 eV for CrO_2(100), shown in Fig. 3.6, are consistent with the results from core emission. The film again demonstrates considerable sensitivity toward the initial sputter. Valence features become more pronounced and the onset of emission shifts away from the Fermi level. Annealing the sputtered film at 450º C in oxygen results in a shift of the onset back toward the Fermi level. The phenomenon of the spontaneous shift of valence features away from the Fermi level after sputtering is often observed in CrO_2 studies and remains unexplained. A suspect for the low polarization yield of CrO_2 based devices is the presence of hydrocarbons at the surface. Slight oxygen peaks are visible near higher binding energies suggesting contamination from crystal growth, atmospheric exposure, and/or vacuum apparatus.

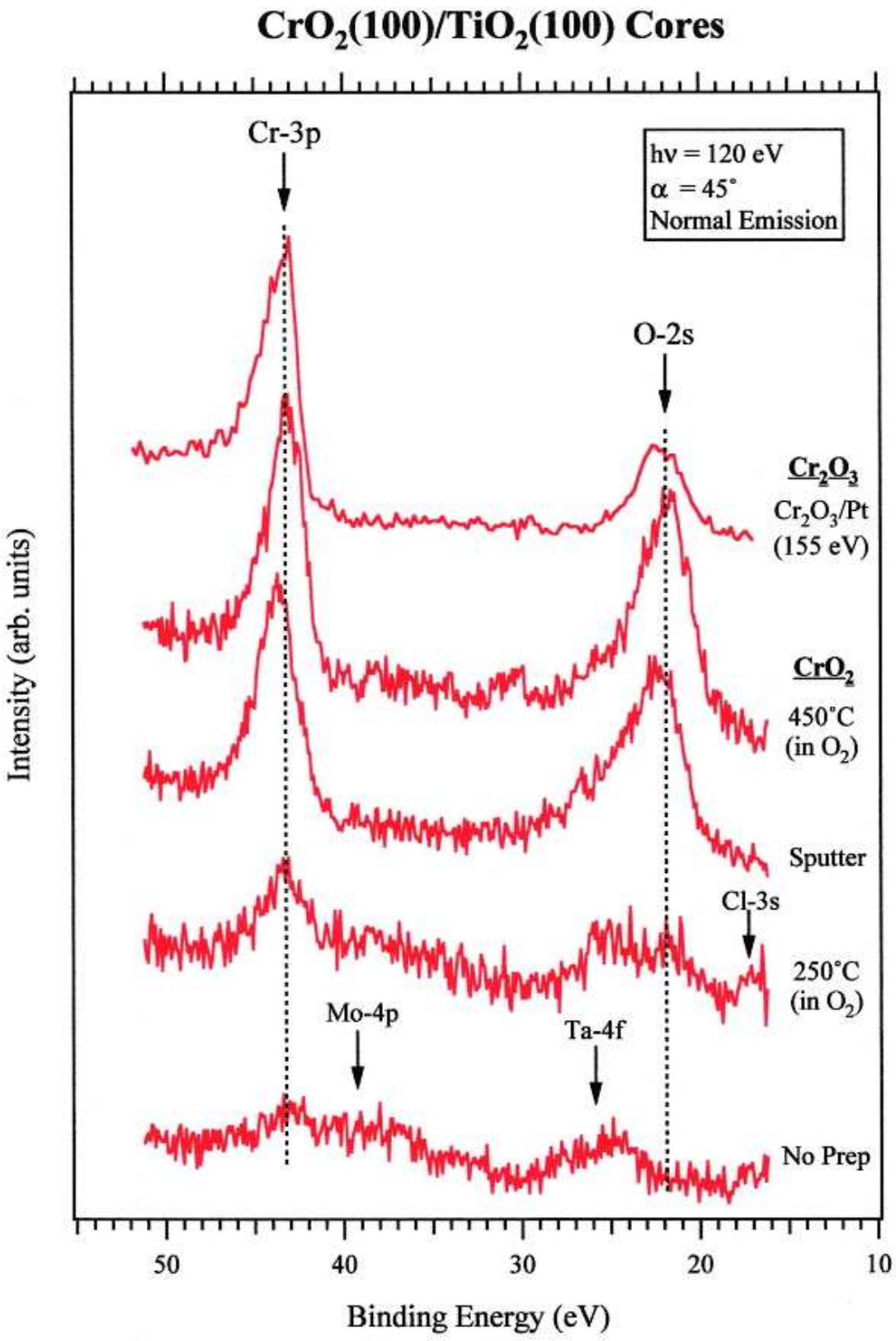

Fig. 3.5 *CrO_2(100) core electron spectra*

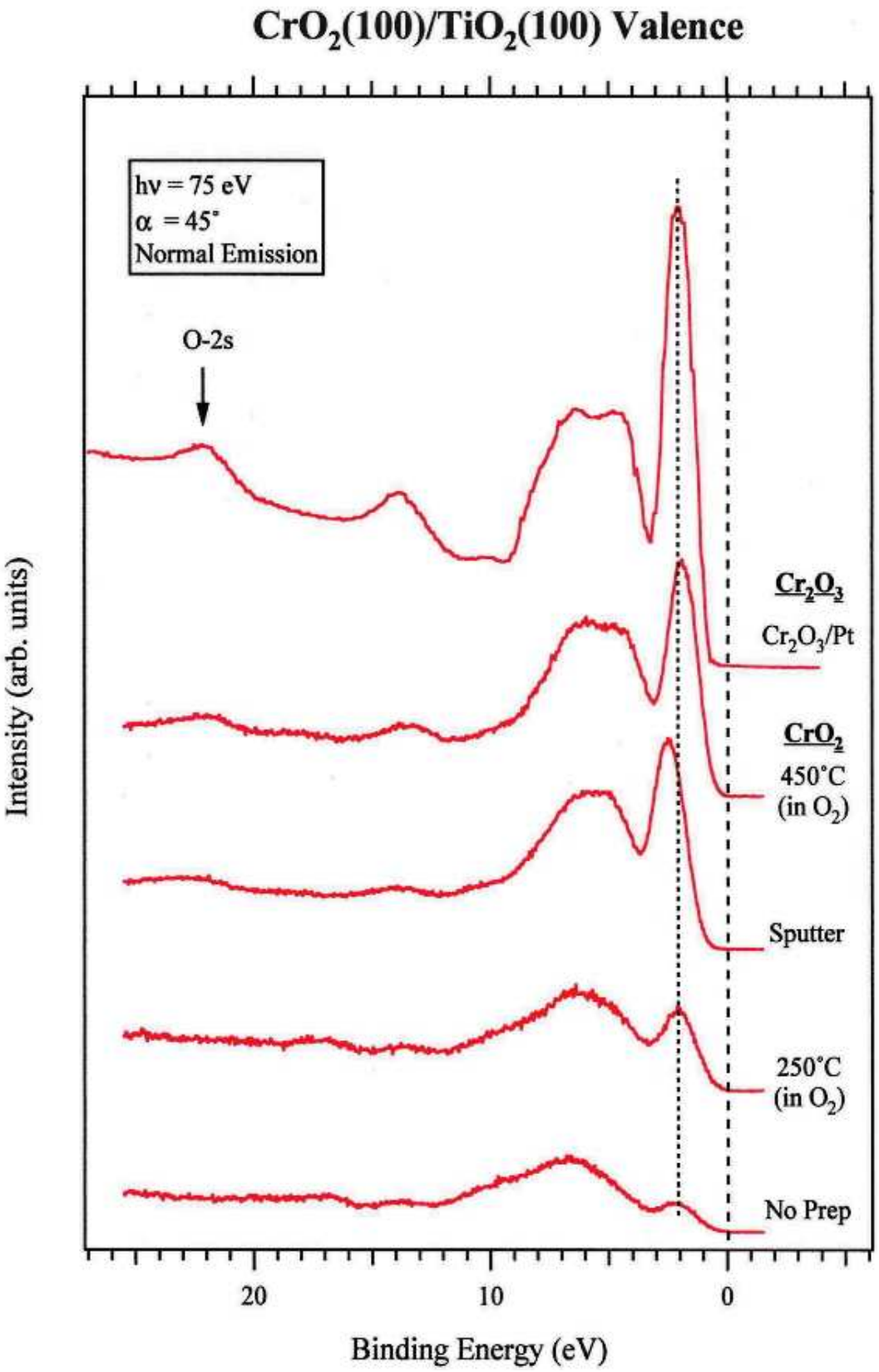

Fig. 3.6 *CrO_2(100) valence electron spectra*

3.2.2 CrO_2(110)

The core electron emission measurements for CrO_2(110) are shown in Fig. 3.7. The oxygen and chromium ratios are preserved throughout the initial sputter and three subsequent annealing processes. Tantalum is detected throughout the entire sample preparation, and chlorine becomes visible after annealing at 450º C, and is even more prevalent after annealing at 600º C. Chromium and oxygen detection reduces after the high temperature annealing at 600º C, but the aspect ratio is conserved. Residual chlorine emission from the liquid precursor becomes more frequent after each anneal, as a result of being driven into the surface film.

Valence emission shown in figure 3.8 indicates the presence of hydrocarbons and chlorine throughout sample preparation. The film shows sensitivity toward sputtering, and annealing at 600º C reduces the chromium and oxygen electron emission, as with the core analysis. As opposed to the CrO_2(100) orientation, the valence features of CrO_2(110) do not seem to shift after the initial sputter. The CrO_2(110) orientation too exhibits insulating qualities with a valence electron emission peak approximately 2 eV below the Fermi level.

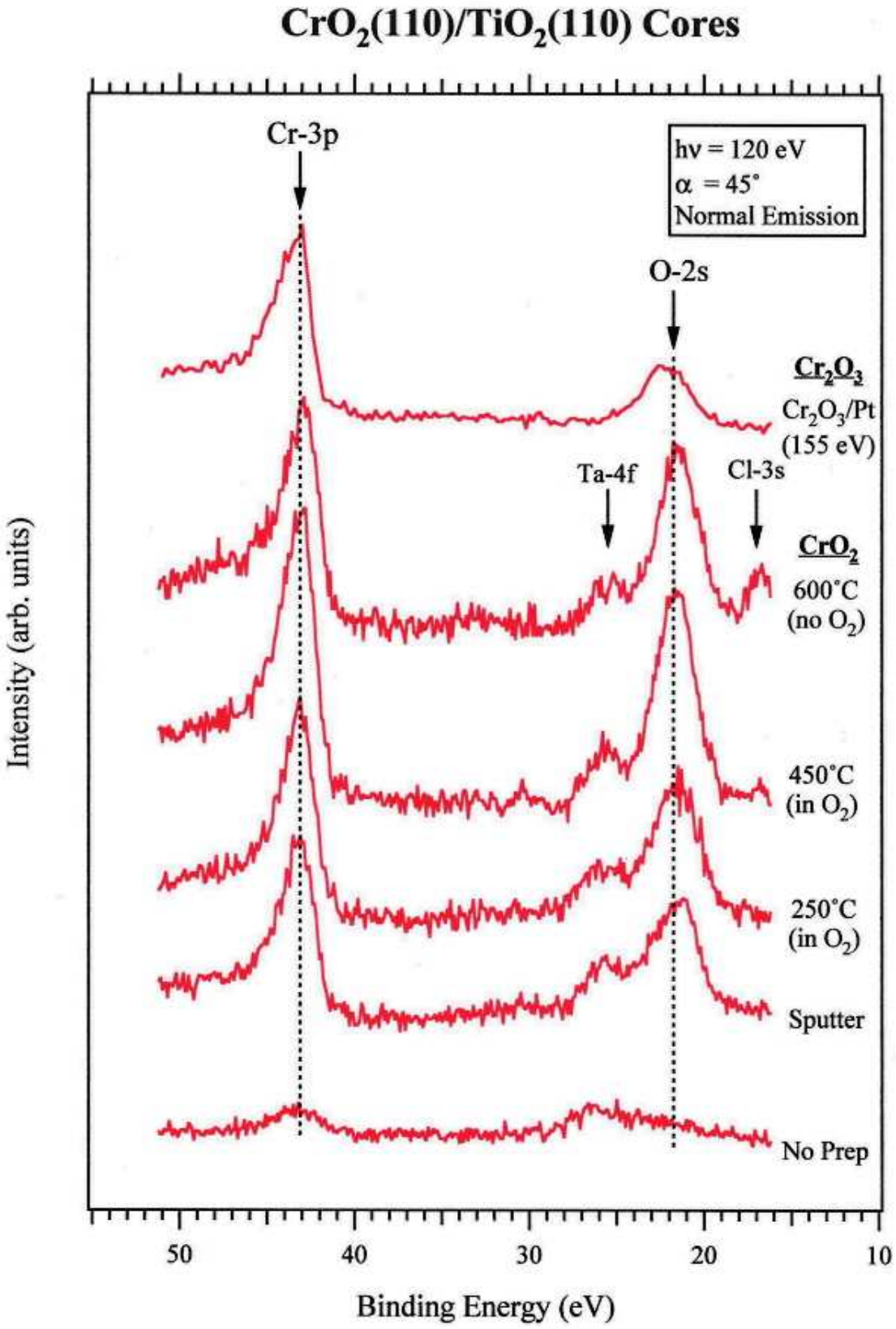

Fig. 3.7 *CrO_2(110) core electron spectra*

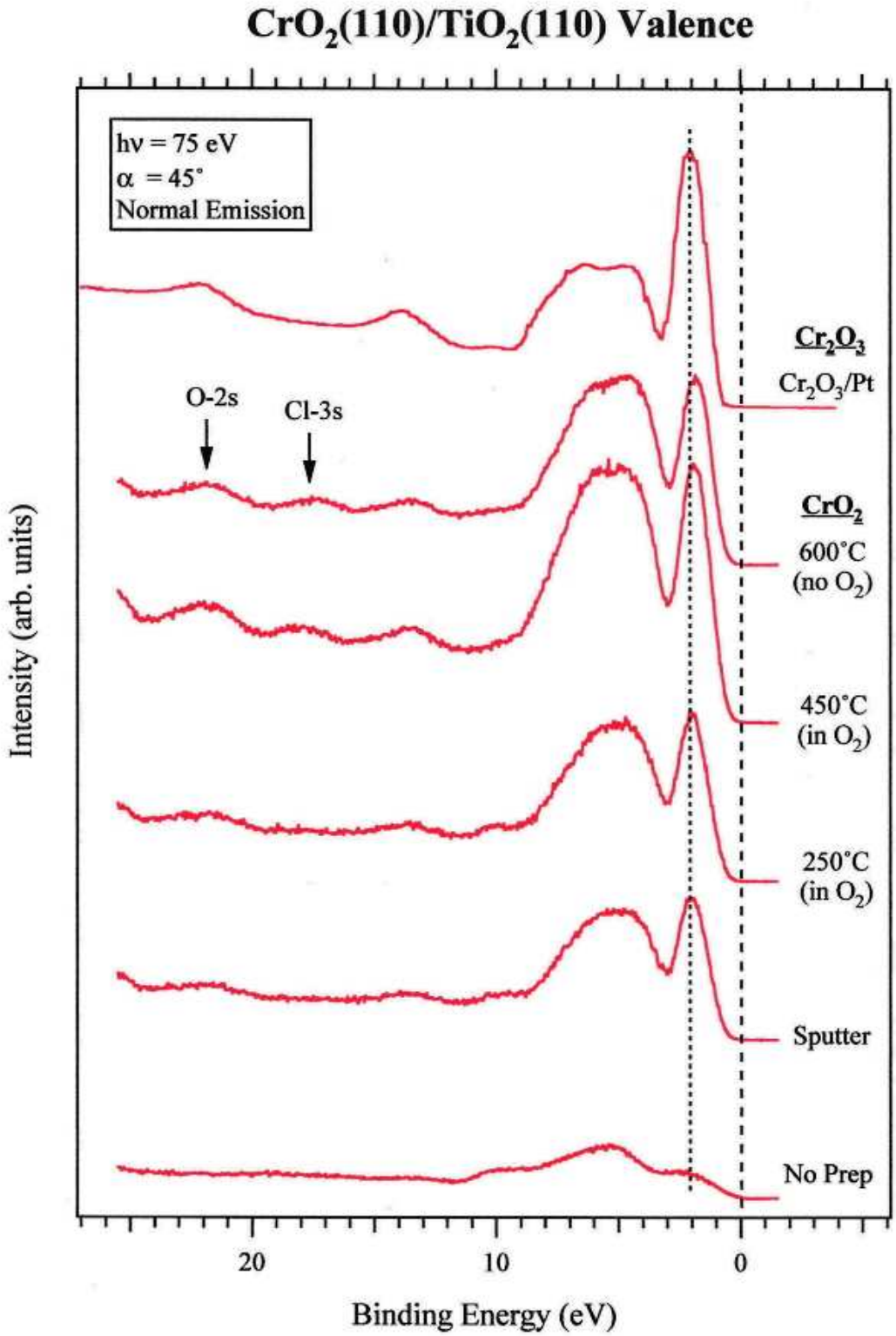

Fig. 3.8 *CrO_2(110) valence electron spectra*

3.2.3 Dry Scroll Pump

Spectra taken with an oil-free dry scroll pump in place of the turbo pump are included in figure 3.9. Intensity levels are comparable to previous results, suggesting that the presence of hydrocarbons is not due to the turbo pump or vacuum apparatus, and is a result of atmospheric exposure or crystal growth. It does not appear that the vacuum was responsible for the hydrocarbon contamination detected on the films being studied. Despite sample preparation, the spectra indicate a nonconductive CrO_2 form with a valence electron concentration approximately 2 eV below the Fermi level, and no electron detection above the Fermi level.

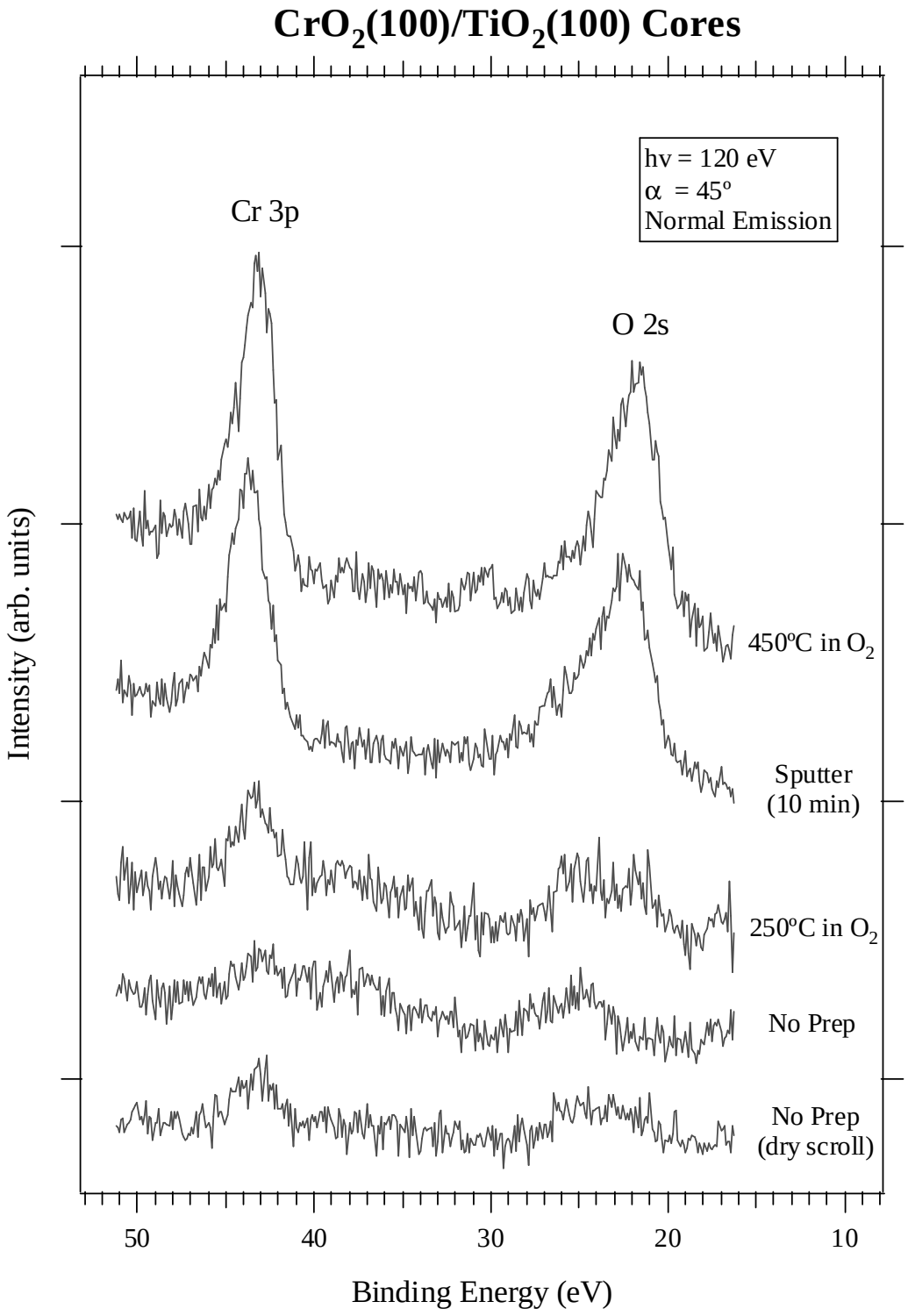

Fig. 3.9 *CrO_2(100) core electron spectra with dry scroll pump*

3.3 CrO_2 LEED

LEED results provide additional evidence for the CrO_2 phase. The diffraction pattern created by the chromium oxide film after annealing at 600º C is shown in Fig. 3.10. The pattern reveals the rectangular symmetry corresponding to the rutile structure of CrO_2(110) illustrated in figure 3.11.

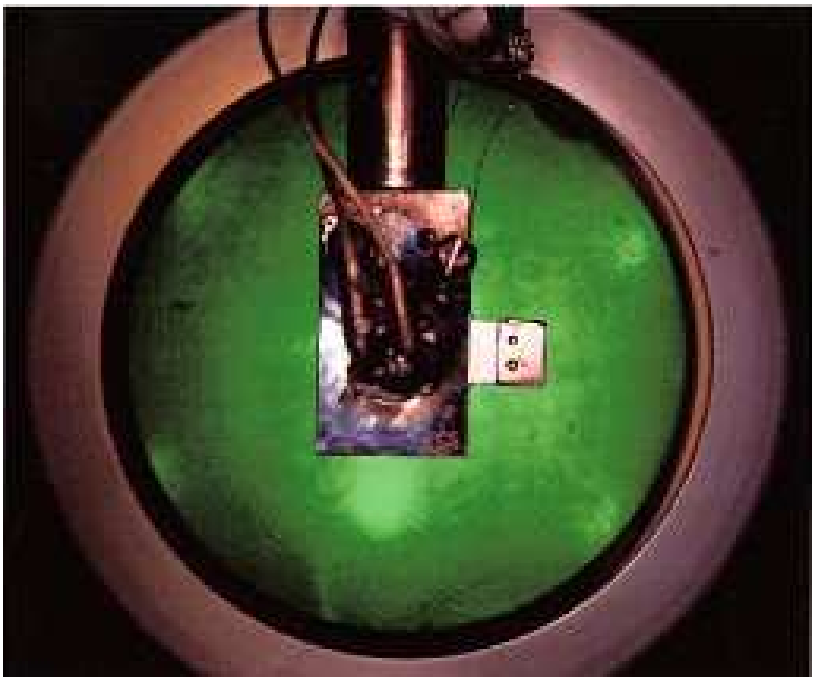

Fig. 3.10 *LEED - CrO_2(110) after 600º C anneal*

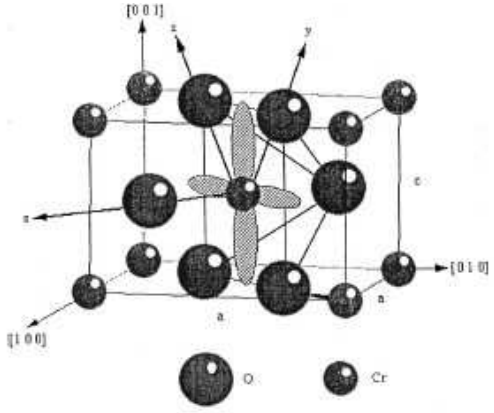

Fig. 3.11 *The rutile structure of CrO_2 [8]*

3.5 Chromium Oxide Density of States Integration

3.5.1 Integration Procedure

As mentioned earlier, comparing the ratio of elements for known and unknown chromium oxide states is a useful method for determining the molecular phase of the film. The relative number of states of chromium and oxygen is determined by integrating the peaks in the core electron density of states spectra. Since the light source is capable of penetrating farther into the surface than the mean free path of the primary electrons, a background signal due to inelastic scattering of these secondary electrons is generated, onto which the primary signal is added. Thus, the secondary signal must be subtracted before integrating the peaks. The procedure used is outlined below.

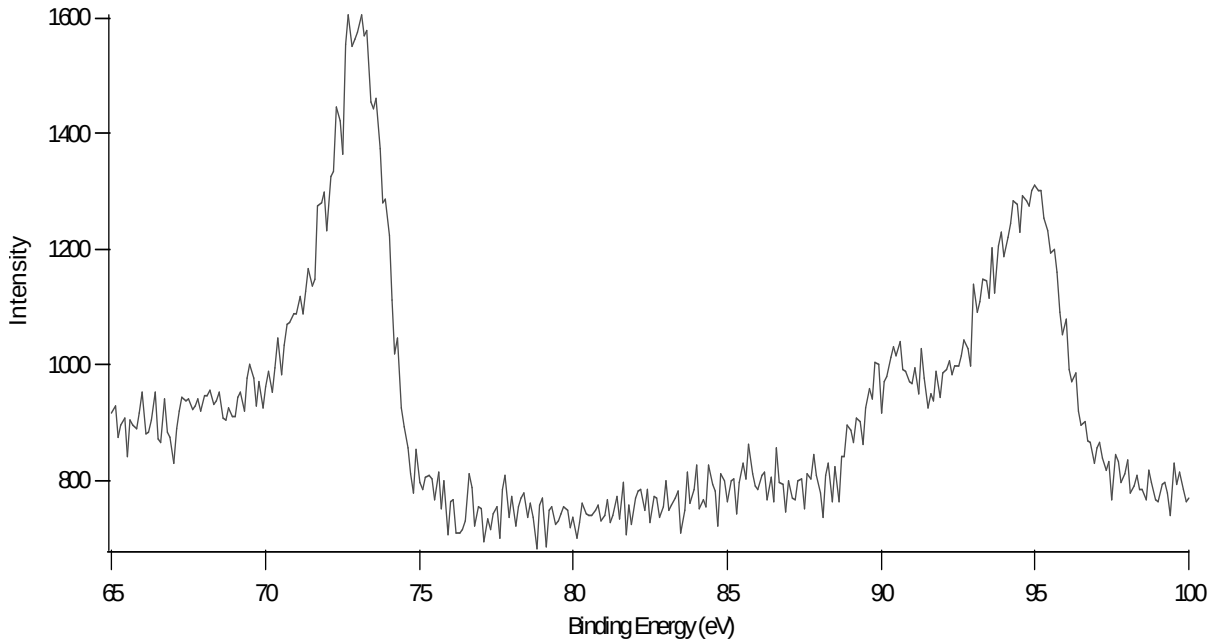

Fig. 3.12 *Actual CrO_2(100) core electron spectrum*

An actual spectrum obtained for CrO_2 grown on TiO_2 is illustrated in figure 3.12. First, the peaks are removed from the data to prepare the spectrum for a polynomial fit of the secondary electron tail.

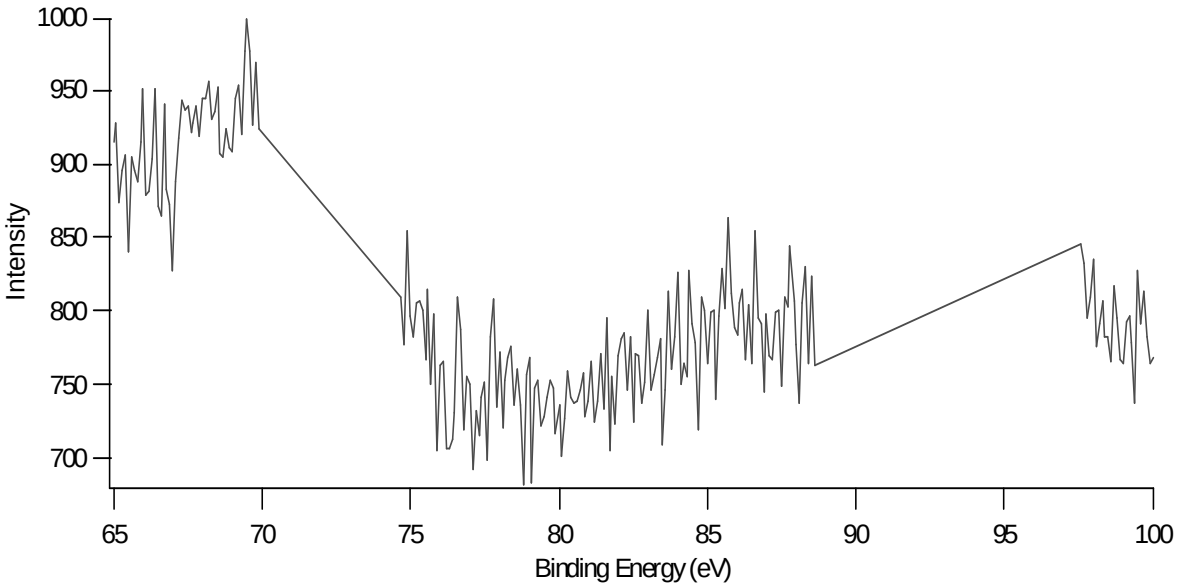

Fig. 3.13 *CrO_2(100) core electron spectrum after peak removal*

A third order polynomial is then fit to the data to approximate the background signal. The polynomial fit is shown by the smooth line running through the data in figures 3.14 and 3.15. The original data with the background signal approximation is displayed in Fig. 3.15.

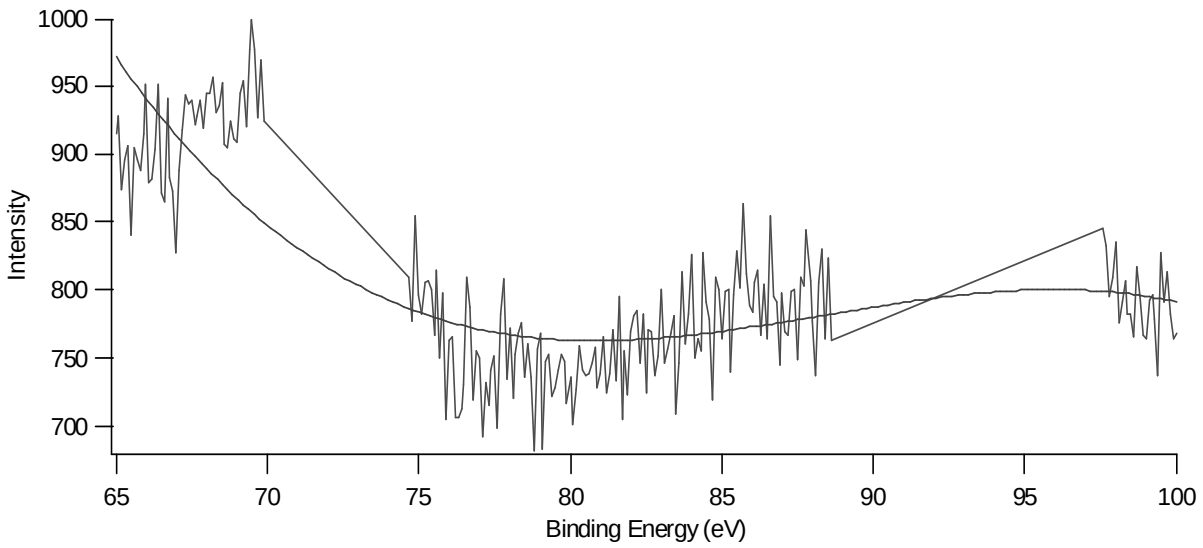

Fig. 3.14 *CrO_2(100) core electron background signal with polynomial fit*

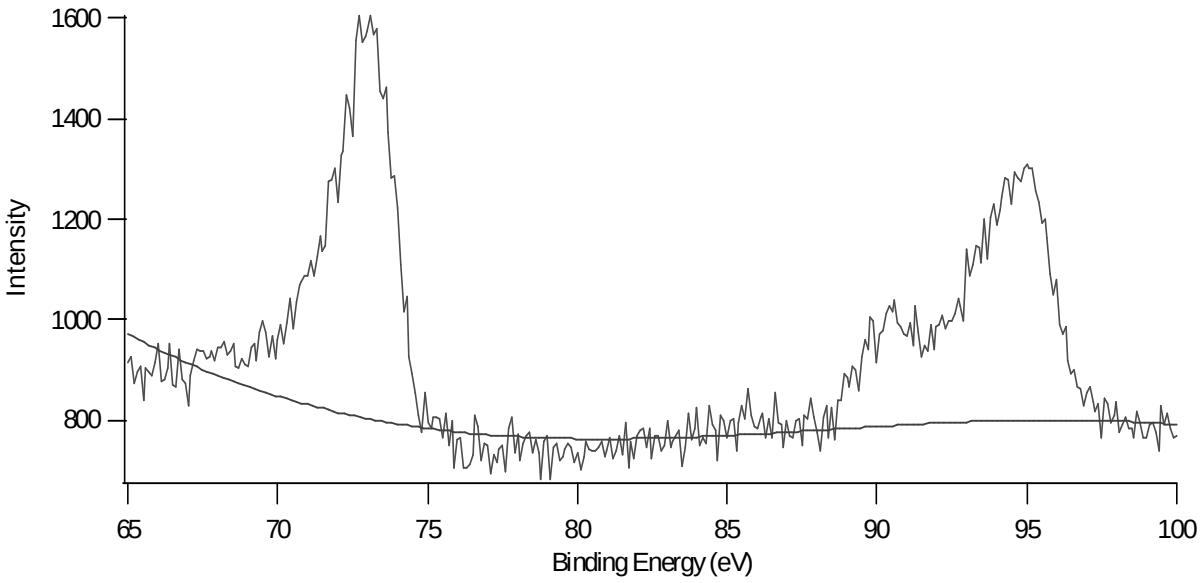

Fig. 3.15 *Actual CrO_2(100) core electron spectrum with polynomial fit*

The primary core electron density of states signal, after subtracting the background signal from the original data is shown in Fig. 3.16. Peak integration can now be performed to determine the oxygen to chromium ratio of the primary electron signal representing the epitaxial film.

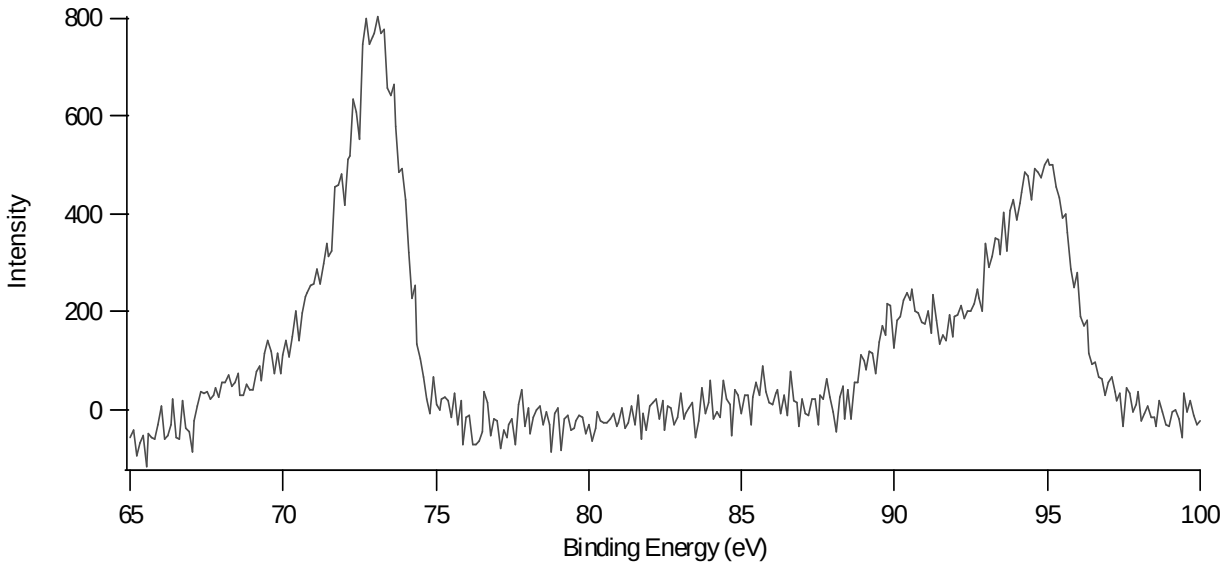

Fig. 3.16 *CrO_2(100) core electron spectrum primary signal*

The following Matlab script integrates the peaks and outputs the ratio of oxygen to chromium states. The script uses a center-bound rectangular integration method of averaging successive intensity values and generating rectangles followed by a summation.

```
%  Daniel Borst
%  peak_spec - Program to integrate and compare spectrum peaks

clc;  help peak_spec;   % Clear command window and print header

%  Initialize parameters
kinetic_e = input('\n\nEnter kinetic energy variable: ');
raw_counts = input('Enter raw counts variable: ');

dt = kinetic_e(2) - kinetic_e(1);   % Define rectangle width

% Plot raw counts vs. kinetic energy
plot(kinetic_e,raw_counts);

%  Isolate chromium peak
l_bound1 = input('\n\nEnter chromium left boundary: ');
r_bound1 = input('Enter chromium right boundary: ');

%  Isolate oxygen peak
l_bound2 = input('\nEnter oxygen left boundary: ');
r_bound2 = input('Enter oxygen right boundary: ');

Cr_total = 0;   % Initialize chromium total states

i = 1;

%  Move to left boundary of chromium
while kinetic_e(i) < l_bound1
    i = i+1;
end

%  Integrate chromium peak
while kinetic_e(i) < r_bound1
    inc = ((raw_counts(i+1) + raw_counts(i))/2)*dt;
    Cr_total = Cr_total + inc;
    i = i+1;
end

O_total = 0;    % Initialize oxygen total states

%  Move to left boundary of oxygen
while kinetic_e(i) < l_bound2
    i = i+1;
end

%  Integrate oxygen peak
while kinetic_e(i) < r_bound2
    inc = ((raw_counts(i+1) + raw_counts(i))/2)*dt;
    O_total = O_total + inc;
    i = i+1;
end

ratio = O_total/Cr_total;   % Oxygen to chromium ratio

%  Output oxygen to chromium ratio
fprintf('Ratio (oxygen/chromium) is %f\n\n ', ratio);
```

3.5.2 Peak Integration Ratios and Phase Determination

The following table shows the results of the peak integrations performed using the procedure described above.

Description	Oxygen to Chromium Ratio	Phase
CrO_2(100) initial sputter	1.1	CrO_2
CrO_2(100) 450º C anneal in O_2	1.1	CrO_2
CrO_2(110) initial sputter	1.0	CrO_2
CrO_2(110) 250º C anneal in O_2	1.1	CrO_2
CrO_2(110) 450º C anneal in O_2	1.1	CrO_2
CrO_2(110) 600º C anneal (no O_2)	0.9	CrO_2

Table 3.1 *Phase determination of chromium oxide film*

The phase is determined by comparing the oxygen to chromium ratio to the known state, such as that after the initial sputter. Both orientations remain in the CrO_2 phase throughout the investigation, even after a high temperature anneal of CrO_2(110). Cr_2O_3 grown on platinum is included for comparison, having an oxygen to chromium ratio of less than half of the CrO_2 data.

4. CONCLUSIONS

Experimental results show high sensitivity toward sputtering with 500 eV Ar^+ and effective removal of surface contaminants, as does the onset of emission for the CrO_2 (100) film. Sputtering and annealing cycles preserve the CrO_2 stoichiometry, but did not produce a "metallic" film. The films also reveal the presence of chlorine, as a result of the CVD growth. Ultimately, evidence suggests that the films exhibit an insulating nature, despite remaining in the CrO_2 phase, and that atmospheric exposure or the CVD growth process is responsible for diminished conductance.

REFERENCES

[1] Newton, R. E. I., *Wave Physics*, Routledge, Chapman and Hall, Inc., (1990).

[2] Zangwill, Andrew, *Physics at Surfaces*, Cambridge University Press (1988).

[3] Burns, Gerald, *Solid State Physics*, Academic Press, Inc. (1985).

[4] Ertl, G., Küppers, J., *Low Energy Electrons and Surface Chemistry*, VCH (1985).

[5] Kittel, Charles, *Introduction to Solid State Physics*, John Wiley & Sons, Inc. (1996).

[6] Hüffner, S., *Photoelectron Spectroscopy*, Springer-Verlag (1996).

[7] Ashcroft, Neil W., *Solid State Physics*, Holt, Rinehart and Winston, (1976).

[8] J. M. D. Coey, M. Venkatesan, *Journal of Applied Physics*, Vol. 91, No. 10, 8345-8347 (2002).

[9] A. Anguelouch, A. Gupta, Gang Xiao, D. W. Abraham, Y. Ji, S. Ingvarsson, C. L. Chien, *Physical Review B*, Vol. 64, 180408-1(R), (2001).

[10] P. S. Robbert, H. Geisler, C. A. Ventrice, Jr., J. van Ek, S. Chaturvedi, J. A. Rodriguez, M. Kuhn, U. Diebold, *Novel electronic and magnetic properties of ultra-thin chromium oxide films grown on Pt(111)*, J. Vac. Sci. Tech. A 16, 990-995 (1998).

[11] Loeb, Leonard B., *The Kinetic Theory of Gases*, Dover Publications, Inc., (1961).

[12] Hecht, Eugene, *Optics*, 4th ed., Addison Wesley, (2002).

[13] R. K. Zheng, H. Liu, Y. Wang, and X. X. Zhang, *Cr_2O_3 surface layer and exchange bias in an acicular CrO_2 particle*, Appl. Phys. Lett. 84, 702-704 (2004; J. Dai, J. Tang, H. Xu, L. Spinu, W. Wang, K. Wang, A. Kumbhar, M. Li, and U. Diebold, *Characterization of the natural barrier of intergranular tunnel*

junctions: Cr_2O_3 surface layers on CrO_2 nanoparticles, Appl. Phys. Lett. 77, 2840-2842 (2000).

[14] H. Holloway, J. C. Anderson, *The Use of Thin Films In Physical Investigations*, Academic Press Inc., (1966).

VITA

Daniel Borst was born in September 1980 in Berrien Springs, Michigan and received his B.A. in electrical engineering from Purdue University. He conducted his graduate work in physics under the advisory of Dr. Carl A. Ventrice, Jr. at the University of New Orleans, and performed his research at CAMD at Louisiana State University. He plans to continue his academic career in physics, and hopes to eventually settle into a research position.